Sub-Saturn Planet MOA-2008-BLG-310Lb: Likely To Be In The Galactic Bulge

A Senior Honors Thesis

Presented in Partial Fulfillment of the Requirements for graduation *with research distinction* in Astronomy in the undergraduate colleges of The Ohio State University

by

Julia A. Janczak

The Ohio State University

May 2009

Project Advisor: Professor Richard Pogge, Department of Astronomy

ABSTRACT

We report the detection of sub-Saturn-mass planet MOA-2008-BLG-310Lb and argue that it is the most likely candidate yet for a bulge planet. Deviations from the single-lens fit are smoothed out by finite-source effects and so are not immediately apparent from the light curve. Nevertheless, we find that a lens model in which the primary has a planetary companion is favored by $\Delta\chi^2 = 880$. Detailed analysis yields a planet/star mass ratio $q = (3.3 \pm 0.3) \times 10^{-4}$ and an angular separation between the planet and star within 10% of the angular Einstein radius. Using color-magnitude data from the source, we are able to constrain the distance to the lens D_L to be $D_L > 6.0\,\mathrm{kpc}$ if it is a star ($M_L > 0.08\,M_\odot$). This is the only host discovered so far that must be in the bulge if it is a star. Analysis of the blended light associated with the event (most likely from the lens but possibly a companion to the lens or source) allows us to estimate the mass of the lens, $M_L = 0.69 \pm 0.14\,M_\odot$. Within 10 years the lens will be separated from the source by $\sim 54\,\mathrm{mas}$. Thus the source of the excess light will likely be detectable by direct observation. At that time, it will be possible to determine unambiguously whether the lens and its planet are in the bulge.

1. Introduction

The gravitational field of a star deflects light passing through it like a lens. When a foreground lens star is aligned with a background source star, the source becomes temporarily magnified. The geometry of a typical microlensing event is shown in Figure 1. The light curve for a simple microlensing event involving two stars has a smooth, symmetric peak. Detecting such rare alignments requires large sky surveys to monitor millions of stars per night in the densely populated region of the Galactic bulge. These surveys generally detect several hundred microlensing events per year, which may then be monitored by follow-up groups like the Microlensing Follow Up Network (μFUN). μFUN is a collaboration of professional and amateur astronomers from across the globe, based at The Ohio State University, that is engaged in searching for planets orbiting the lens stars in microlensing events. Such planets create caustic lines, closed contours in the lens that highly magnify the source as it passes through. A caustic crossing creates short perturbations in the light curve that indicate the presence of a planet.

Over the past 5 years, microlensing has led to the discovery of several exoplanets that would not be detectable by any other method currently available. Because it does not rely on light coming from the planet or the host star, microlensing is able to detect planets at several

kiloparsecs, probing even into the center of our Galaxy. Thus microlensing has the potential to determine the demographics of planets orbiting stars from two distinct stellar populations, bulge stars and disk stars. This is critical for understanding the Galactic distribution of planets and may allow us to constrain the time-history of planet formation in the universe. The radial velocity and transit planet detection methods have effectively probed the region of parameter space within the Snow Line, the distance from the host star at which ice can form (see Fig. 2). Over 300 planets have been discovered using these methods. The nine microlensing planet detections to date have probed a region largely unexplored beyond the snow line, where the condensation of icy cores is thought to play an essential role in the formation of gas giants (Pollack et al. 1996). Thus microlensing may also provide us with valuable insight to processes of planet formation.

Standard models of the spatial and velocity distributions of stars in the Galaxy predict that roughly 2/3 of all microlensing events of stars in the bulge arise from bulge lenses, i.e., stars in the bulge (Kiraga & Paczyński 1994). In light of this, one might expect that planetary detections via microlensing would be more frequent in the bulge than in the disk. On the contrary, of the eight other microlensing planets discovered so far (Bond et al. 2004; Udalski et al. 2005; Beaulieu et al. 2006; Gould et al. 2006; Gaudi et al. 2008; Bennett et al. 2008; Dong et al. 2008), five have measured or constrained lens distances, and all five of these distances place the planets in the foreground disk. The distance is not well constrained for the remaining three planets (OGLE-2005-BLG-169Lb, OGLE-2005-BLG-390Lb, and OGLE-2007-BLG-400Lb), and none have been definitively identified as bulge planets. The low detection rate of bulge planets may arise from a selection bias that favors the longer events that preferentially arise from disk lenses, or it may reflect the underlying Galactic distribution of planets. Here we present the analysis of a planetary signature in microlensing event MOA-2008-BLG-310, the best candidate for a bulge planet to date.

2. Observations

The Microlensing Observations in Astrophysics (MOA) collaboration detected microlensing event MOA-2008-BLG-310 [(RA,Dec)=(17:54:14.53,-34:46:40.99), (l,b)=(355.92,-4.56)] on 6 July 2008 ($\mathrm{HJD}' \equiv \mathrm{HJD} - 2450000 = 4654.458$). MOA issued a high-magnification alert two days later, about 12 hours before the event peaked. The color and magnitude of the source indicate that it is a G type star in the Galactic bulge, a result confirmed by high-resolution spectroscopy (Cohen, et al. 2009).

(μFUN) began to intensively monitor this event at $\mathrm{HJD}' = 4656.026$, less than 9 hours before the peak. The minimum predicted peak magnification was $A_{\mathrm{max}} > 80$ but the best-fit

model at the time was consistent with infinite magnification, so the event was given high priority. Observations were taken by five observatories, MOA (New Zealand) 1.8m I, μFUN Auckland (New Zealand) 0.41m R, μFUN Bronberg (South Africa) 0.36m unfiltered, μFUN SMARTS CTIO (Chile) 1.3m I, V, H, and MiNDSTEp La Silla (Chile) 1.54m I. Only one observatory, μFUN Bronberg, was positioned to see the peak of the event. Nevertheless this observatory provided very complete coverage. μFUN Bronberg took a total of 973 observations over the period $4656.21 < \mathrm{HJD}' < 4656.55$, recording the peak and all interesting anomalies. The high density of these observations allows us to bin the μFUN Bronberg data without compromising the time resolution. The binned datapoints (as seen in Fig. 3) occur every 2.5 minutes over the peak, whereas each planetary feature spans roughly an hour. μFUN SMARTS took a total of 49 images in the I-band, 275 images in the H-band, and 6 in the V-band. The μFUN SMARTS observations overlap μFUN Bronberg by about 2 hours, starting after the peak and providing additional coverage of the last planetary deviation.

MOA data were reduced using the standard MOA difference imaging analysis pipeline. For our analysis of the lightcurve, we primarily use DIA (Woźniak 2000) reductions of data from μFUN observatories. We also use DoPhot (Schechter et al. 1993) reductions of μFUN SMARTS H-band data to investigate the light that is blended with the source. The error bars for the data points are renormalized so that χ^2 per degree of freedom for the best fit binary-lens model is close to unity.

Because they are unfiltered, the μFUN Bronberg data require a differential extinction correction because the source has a different color than the mean color of the reference frame used by DIA. We measure this effect from the "light curves" of stable stars having the same color as the lens, and thereby remove it. See Dong et al. (2009).

3. Microlens Model

MOA-2008-BLG-310 was initially modeled as a single lens event. The single-lens model light curve fits the data reasonably well, showing pronounced finite-source effects in the rounding of the peak but no obvious anomalies. The event reached a maximum magnification $A_{\rm max} \sim 400$, making it a good candidate for planet detection although the finite-source effects work to smooth out any planetary deviations. Figure 3 shows the best-fit single-lens model. The model allows us to roughly determine several parameters pertaining to the general structure of the light curve; $t_0, u_0, t_{\rm E}$, and ρ. Here, t_0 is the time of minimum separation between the source and lens, u_0 is the minimum separation in units of the Einstein radius, ρ is the radius of the source in the same units, and $t_{\rm E}$ is the Einstein crossing time. We find that the source crossing time, $t_* \equiv \rho t_{\rm E}$, is better constrained than ρ, and so we report this

parameter as well.

A close look at the residuals from the single-lens fit reveals significant structure indicating that the underlying lens model is more complicated than a simple single lens. In particular, short timescale deviations near the peak of high-magnification events are typically caused by planetary or binary companion. In these cases, the caustic structure is extended, as opposed the a simple point in the case of an isolated lens, leading to deviations from the single-lens form as the source crosses the caustic. A short spike in the residuals just before the peak and a short dip just after are completely covered by unfiltered observations from μFUN Bronberg. The second of these features is confirmed in I-band data from μFUN SMARTS. SMARTS H-band observations qualitatively show the same deviation despite suffering from large scatter. Since the higher quality I-band data cover the same portion of the light curve, H-band data are not used in the derivation of model parameters.

The relatively low amplitude of the residuals from a single-lens model, along with the fact that these residuals are apparent over most of the duration of the source diameter crossing, generally indicate that the central caustic structure due to the binary companion is only magnifying a fraction of the source at one time (Griest & Safizadeh 1998; Han 2007). This suggests that w, the "short diameter" or "width" of the central caustic is smaller than the diameter of the source (see Chung et al. 2005). Prominent deviations from the single-lens model occur where the limb of the source enters and exits the caustic. This behavior, which is qualitatively very similar to that of MOA-2007-BLG-400 (Dong et al. 2008), prompts us to investigate possible binary-lens models.

3.1. Searching a Grid of Lens Geometries

Using the method of Dong et al. (2008), the initial search for binary solutions is conducted over a grid of three parameters: the short-caustic width w, companion/star mass ratio q, and the angle of the source trajectory relative to the binary axis α. Since w is a function of q and the companion/star separation d, this is equivalent to also fixing d at various values. The remaining parameters (t_0,u_0,$t_{\rm E}$,ρ) are allowed to vary. Two additional parameters for limb darkening are given fixed values, as will be discussed in § 4. We use Monte Carlo Markov Chain (MCMC) to minimize χ^2 at each of the (w, q, α) grid points. There is a well known degeneracy such that for $q \ll 1$, planet/star separations d and d^{-1} will produce almost identical central caustic structures and consequently indistinguishable light curves for high magnification events such as this (Griest & Safizadeh 1998). We explore a (w, q) grid for each geometry, searching the $d \geq 1$ (in units of the Einstein radius) regime for 'wide' solutions and the $d < 1$ regime for 'close' solutions.

3.2. Best-Fit Model

An initial search for binary solutions is conducted over the range of caustic widths $-3.5 \leq \log w \leq -1.5$ (in units of the Einstein radius), companion mass ratios $-5.0 \leq \log q \leq 0$, and source trajectory angles $0 \leq \alpha \leq 2\pi$ in the two separate regimes $d \geq 1$ and $d < 1$. This initial search gives us fairly good estimates of the best-fit parameters and the location of the χ^2 minima in terms of w and q (also d). For this particular event, however, w and q turn out to be highly correlated. We conduct a refined search over a grid in (d, q) instead of (w, q), and we also allow α to vary as a MCMC variable, rather than discretely. The solid black lines in Figure 4 show $\Delta\chi^2 = 1, 4, 9$ contours in the (d, q) plane for the wide (*top*) and close (*bottom*) solutions, respectively. For the wide solution, the χ^2 minimum occurs at $d = 1.084 \pm 0.003$ and $q = (3.31 \pm 0.26) \times 10^{-4}$. The close solution minimum occurs at $d = 0.927 \pm 0.003$ and $q = (3.31 \pm 0.26) \times 10^{-4}$. The mass ratio indicates that the companion to the lens is in fact a planet. As expected, we recover the $d \leftrightarrow d^{-1}$ degeneracy. The wide solution is favored by just $\Delta\chi^2 = 1.61$, indicating that the wide/close degeneracy cannot be clearly resolved in this case. The best-fit parameters for both wide and close solutions are recorded in Table 1.

The wide and close planetary models qualitatively explain several features of the single-lens residuals. The lower panel of Figure 5 shows the extended source at key points in time on its trajectory. The nearly identical central caustics generated by the best-fit wide and close models both shown. The most prominent features in the residuals, shown in the upper panel of Figure 5, occur as the limb of the source crosses the caustic. The positive and negative spikes that are most evident from the raw data (features 2 and 4 of Fig. 5) coincide with the limb of the source entering the strong curved portion of the caustic and exiting the weaker straight segment. The bottom panel of Figure 3 shows the residuals to the best-fit wide binary model. The deviations from the point-lens model that initially indicated that the lens was not being accurately modeled are no longer apparent. The planetary model decreases χ^2 by 880, making this a strong detection of a Saturn mass-ratio planet/star system.

Table 1. MOA-2008-BLG-310 Best-Fit Close and Wide Planetary Model Parameters

	d	q	t_0(HJD')	u_0	$t_{\rm E}$(days)	α(rad)	t_*(days)
Close	0.927	3.31×10^{-4}	4656.3998	3.047×10^{-3}	10.97	1.212	0.05486
Wide	1.084	3.31×10^{-4}	4656.3997	3.046×10^{-3}	10.98	1.211	0.05482

4. Limb Darkening

Since the primary deviations in the light curve occur at the limb of the star, it is important to examine the effects of limb darkening on the planetary solution. For this purpose we adopt a surface brightness profile of the form

$$\frac{S(\vartheta)}{S_0} = 1 - \Gamma\Big[1 - \frac{3}{2}(\cos\vartheta)\Big] - \Lambda\Big[1 - \frac{5}{4}(\cos^{1/2}\vartheta)\Big], \tag{1}$$

where ϑ is the angle between the normal to the surface of the star and the line of sight (An et al. 2002). Since μFUN Bronberg provided the bulk of the observations covering the peak of the event and the deviations at the limb of the source, it is most critical that the limb darkening be accurately modeled for these data. Using the method previously outlined, Γ and Λ are allowed to vary for Bronberg data along with parameters $t_0, t_{\rm E}, u_0, \rho$, and α in searching the (d, q) grid. The best-fit models for wide and close planet/star separations have $(\Gamma, \Lambda) = (-0.200, 1.277)$ and $(\Gamma, \Lambda) = (0.069, 0.732)$ respectively. To determine whether these values are consistent with standard limb darkening models we compare our results to $(\Gamma, \Lambda) = (0.166, 0.543)$ corresponding to $(c, d) = (0.204, 0.557)$ from Claret (2000) for R band. These parameters pertain to a star with $T_{\rm eff} = 5750\,{\rm K}$ and $\log g = 4.0$, i.e., a post-turnoff G star, corresponding to the $(V - I)_0 = 0.70$ and $M_I = 3.4$ that we derive from the instrumental color-magnitude diagram by assuming that the source suffers the same extinction and is at the same distance as the bulge clump. Although observations from Bronberg are unfiltered, we find that the spectral response is most closely mimicked by R band. That is, from a color-color diagram of stars in the field with colors similar to that of the microlensed source, we find that

$$\Delta(R_{\rm Bron} - I) = 0.50\,\Delta(V - I), \tag{2}$$

i.e., almost exactly what would be expected for standard R band. The surface brightness profile from our free fit is qualitatively similar to Claret (2000). We further investigate limb darkening by fixing the parameters for μFUN Bronberg at the Claret (2000) values for R band while fixing MOA and μFUN SMARTS data at the Claret (2000) values for I band, $(\Gamma, \Lambda) = (0.077, 0.549)$ corresponding to $(c, d) = (0.099, 0.584)$. The $\Delta\chi^2$ contours for the close and wide planetary models with limb darkening fixed at the Claret (2000) values are shown in Figure 4 as the solid black lines. These contours are similar to the dotted red lines in Figure 4 generated by allowing the parameters for limb darkening to vary freely. Most importantly, the best-fit values of d and q change by much less than one sigma. This justifies fixing the parameters for limb darkening at the Claret (2000) values for all models that follow.

5. Measurement of Angular Einstein Radius $\theta_{\rm E}$

The color and magnitude of the source allow us to determine its angular radius θ_*, which in turn can be used to place constraints on the lens mass and lens-source relative parallax. Using standard techniques (Yoo et al. 2004), we begin by measuring the offset of the source relative to the clump centroid, $\Delta[(V-I), I] = (-0.35, 3.62)$ (see Fig. 6). Adopting $[(V-I)_0, I_0]_{\rm clump} = (1.05, 14.32)$ for the dereddened position of the clump then gives us the source color and magnitude $[(V-I)_0, I_0]_s = (0.70, 17.94)$, where the derived I_0 is the same for the close and wide solutions. Converting $(V-I)$ to $(V-K)$ using the color-color relations of Bessell & Brett (1988), we obtain $(V-K)_0 = 1.53$. We use the color/surface-brightness relations of Kervella et al. (2004) to calculate θ_*,

$$\theta_* = 0.81 \pm 0.07\,\mu{\rm as}, \tag{3}$$

which (as with the next three equations) applies equally to both the close and wide solutions. The source crossing time t_* is

$$t_* \equiv \rho t_{\rm E} = 0.05482 \pm 0.00005\,{\rm days}, \tag{4}$$

which implies that the (geocentric) proper motion, $\mu_{\rm geo} = \theta_*/t_*$, is

$$\mu_{\rm geo} = 5.4 \pm 0.5\,{\rm mas\,yr^{-1}} \tag{5}$$

The inferred Einstein radius, $\theta_{\rm E} = \mu_{\rm geo} t_{\rm E}$, is then,

$$\theta_{\rm E} = 0.162 \pm 0.015\,{\rm mas} \tag{6}$$

We can relate the lens mass M_L to the source-lens relative parallax $\pi_{\rm rel}$ (see Gould 2000 for details),

$$M_L = \frac{\theta_{\rm E}^2}{\kappa \pi_{\rm rel}} \tag{7}$$

where $\kappa = 4G/c^2\,{\rm AU} \sim 8.1\,{\rm mas}\,M_\odot^{-1}$. If we require that $M_L > 0.08\,M_\odot$ (that is, if the lens is a star) then it follows that $\pi_{\rm rel} < 41\,\mu$as. Assuming $D_S = 8\,$kpc for the source to be in the bulge, this gives a lower limit on the distance to the lens $D_L > 6.0\,$kpc. We conclude that if the lens mass is above the hydrogen burning limit, then it must be located in the Galactic bulge. In order to verify the bulge location of the lens, we would need another independent relation between the lens mass and distance. This could be obtained by measuring either the microlensing parallax or the flux from the lens.

6. Parallax

Determining the microlensing parallax $\boldsymbol{\pi}_{\rm E}$ gives us a independent relationship between the lens mass and source-lens relative parallax (Gould 2000). The magnitude of the vector is given by,

$$\pi_{\rm E} = \sqrt{\frac{\pi_{\rm rel}}{\kappa M_L}} \tag{8}$$

while the direction is the same as that of $\boldsymbol{\mu}_{\rm geo}$, the lens-source relative proper motion in the geocentric frame. In combination with the independent relation between M_L and $\pi_{\rm rel}$ obtained from the proper motion of the source, it would be possible to give physical values to both of these parameters. With this goal in mind we examine the effects on the light curve from two sources of parallax. Orbital parallax is caused by the acceleration of the Earth on its orbit. Terrestrial parallax arises from two or more widely separated observatories simultaneously observing a slightly different light curve due to their different vantage points. For this event orbital parallax is not expected to be detectable since the timescale is so short ($t_{\rm E} = 10.97$ and 10.98 days for the close and wide models respectively). We expect terrestrial parallax to be poorly constrained as well. Earth-based parallax measurements require that short duration caustic crossings be observed by two or more telescopes simultaneously (Hardy & Walker 1995). While μFUN Bronberg and μFUN SMARTS both observed the second prominent deviation as the limb of the source exited the caustic, this feature is somewhat elongated by finite source effects. We once again search the (d, q) grid, allowing the north and east components of both terrestrial and orbital parallax to vary as additional MCMC parameters. We also test the case of the source-lens minimum separation $u_0 \leftrightarrow -u_0$ as this is a known degeneracy in determining parallax (Smith et al. 2003). For the four cases ($\pm u_0$, close/wide), the reduction in χ^2 ranges from 2 to 7, i.e., barely different from the $\Delta\chi^2 = 2$ expected from reducing the degrees of freedom by 2. The marginal detection of parallax at $\Delta\chi^2 = 7$ favors $\pi_E = 5$. Such a large parallax yields $\pi_{\rm rel} = \pi_E \theta_E = 0.8\,{\rm mas}$ and lens mass $M_L = 0.004\,M_\odot$. We do not give much weight to this possible free-floating planet solution since such small $\Delta\chi^2$ could easily be produced by low-level systematics (Poindexter et al. 2005). Hence we obtain essentially no new information, and, as our results are consistent with zero orbital and terrestrial parallax, we set $\pi_{\rm E} = 0$ hereafter.

7. Blended Light

From the best-fit model we obtain a measure of how much light is being lensed in the event, in other words the flux of the unmagnified source. In addition to the source flux, there is blended light that is not being lensed, which may come from unrelated stars along the line

of sight, companions to the source or lens, or the lens itself. An alternate route to obtaining the lens mass and distance is possible if the flux from the lens can be isolated (Han 2005; Bennett et al. 2007).

We have H-band images of the event taken from CTIO. We have additional post-event JHK Infrared images of MOA-2008-BLG-310 taken with the IRSF telescope in South Africa on 2008 August 4 and the adaptive optics system NACO on the ESO VLT on 2008 July 28. The pixel scales are respectively 0.27, 0.45 and 0.027 arcsec. A log of the observations is given in Table 2. We reduce the IRSF images following standard procedures, and measure the fluxes and positions of stars using the DoPhot software.

The NACO and IRSF images reveal two additional stars in the vicinity of the source that are unresolved by the observations used in the light curve analysis. One of these is 3 mag brighter than the magnified source and 0.85 arcsec away (star 3 in Fig. 7) while the other is 0.2 mag brighter and 0.5 arcsec away. To definitively identify the source from among this group, we create a template image from the best CTIO I-band images and subtract this template from an image near the peak of the event. The magnified light of the source is isolated on the subtracted image because the contribution from other stars is removed. Thus the position of the source is very precisely determined. DoPhot is used to find the positions of other stars on the template CTIO I and median NACO H images. We select 18 isolated stars common to both images and calculate the coordinate transformation from CTIO to NACO. The position of the source transformed to NACO coordinates is 12.7 ± 5 mas from the centroid of the target in Figure 7. The nearest neighboring star is 400 mas from the source position, and thus the identification of the source with the target on the NACO frame is very secure.

Since the NACO images reduction is a delicate procedure, we present it in more detail.

Table 2. Log of Observations

Image	Date	hour	FWHM
$J_{\rm IRSF}$	2008-08-04	18:05:25	1.4 arcsec
$H_{\rm IRSF}$	2008-08-04	18:05:25	1.4 arcsec
$K_{\rm IRSF}$	2008-08-04	18:05:25	1.3 arcsec
$J_{\rm NACO}$	2008-07-28	01:29:20	0.15 arcsec
$H_{\rm NACO}$	2008-07-28	02:18:29	0.16 arcsec
$K_{\rm NACO}$	2008-07-28	00:36:17	0.15 arcsec

The master darks are median stacked from 5 raw dark frames taken on the same night with the same integration time (40 s for H band, 50 s for J and Ks) as the science frames. The master flatfield is obtained from 6 lampflats taken the same night. A badpixel map for correction of the raw frames is obtained using the deadpix routine from the ESO ECLIPSE package (Devillard 1997). The science frames (24 s in J, H and 49 s in Ks) are then dark subtracted, flatfielded, median co-added and sky-subtracted using the JITTER infrared data reduction software (Devillard 1999). To avoid border effects we keep only the intersection of frames for all the dithered positions for our photometric analysis.

We use the Starfinder (Diolaiti et al. 2000) tool to extract the photometry of the reduced NACO frames. Starfinder has been specially designed to perform photometry of AO images of crowded fields. It creates a numerical psf template from chosen stars within frame, which is then used for psf-fitting of all stars in the field. Even though the AO correction for the given data set is good (strehl ratios of around 10%) and the variation of the psf-shape across the field of view is small, we decide to take star 3 (see Fig. 7) as psf template for best photometric accuracy on the target, as it is the closest high signal-to-noise (S/N) star to the microlens.

We perform astrometry in two steps. First, IRSF images are calibrated with respect to 2MASS reference stars using both GAIA/Skycat Fit to obtain initial star positions relative to the 2MASS astrometric catalog and then Tweak is used to refine them. The WCS positions of IRSF objects are deduced using the WCSTools routine xy2sky and used as references to calibrate NACO images with the WCSTools routine imwcs.

7.1. Photometric calibration of IRSF, VLT NACO and H CTIO

Our goal is to put NACO photometry of the target (blend + magnified source) on the CTIO photometric system, so that it can be compared with the source-only H-band flux, which is well-measured by the CTIO H-band photometry during the event. In principle, this could be done using comparison stars common to NACO and CTIO. However, there are only two such stars and they have relatively large photometric errors in CTIO photometry. Instead, we use a large number of common stars to photometrically align the CTIO and IRSF systems, which can therefore be done very accurately. We then align the NACO and IRSF systems based on 4 common stars, which have much smaller errors and consequently show smaller scatter than the CTIO stars.

Specifically, we perform the following steps. First, we cross identify 1521 objects between the 2MASS and IRSF frames, 779 of which have high quality flags (labeled AAA in 2MASS

catalog), and then apply two further restrictions: keeping only the bright end of the sample, and removing 1.5 sigma outliers. We adopt the color terms as given by the IRSF manual and we fit the zero point :

$J_{\rm IRSF,calib} = 23.073 \pm 0.001 + J_{\rm 2MASS} - 0.043(J_{\rm 2MASS} - H_{\rm 2MASS}) + 0.018(adopted) RMS = 0.005$
$H_{\rm IRSF,calib} = 23.128 \pm 0.001 + H_{\rm 2MASS} + 0.015(J_{\rm 2MASS} - H_{\rm 2MASS}) + 0.024(adopted) RMS = 0.005$
$K_{\rm IRSF,calib} = 22.334 \pm 0.001 + K_{\rm 2MASS} + 0.010(J_{\rm 2MASS} - K_{\rm 2MASS}) + 0.014(adopted) RMS = 0.010$

We apply this relation to the 3006 objects with good cross ID in IRSF images. Up to this point, we have calibrated JHK measurements taken by the IRSF telescope. In the NACO field, we identify 6 bright stars likely not to be affected by blending when comparing IRSF and NACO images. Two of them are variable, which leaves us with four stars with the color range $(J-H) = 0.4 - 0.78$. We note that there is no color term in the transformation, and estimate the calibration constant between $H_{\rm IRSF,calib}$ and instrumental NACO to be 27.873 ± 0.014 in H.

We cross-identify 209 stars in the IRSF and CTIO H-band images with matches better than $0.8''$. We clip at ± 0.1 mag around the mean of $H_{\rm CTIO} - H_{\rm IRSF,calib}$, and keep 175 stars. We estimate the zero point offset between instrumental $H_{\rm CTIO}$ and $H_{\rm IRSF,calib}$ to be 3.81638 ± 0.0034.

7.2. Estimation of the target flux in H CTIO

We calibrate the NACO H-band magnitude of the target via the route IRSF-2MASS, $H_{\rm NACO,calib} = 17.47 \pm 0.05$. Using the IRSF-CTIO transformation, we convert the measured NACO flux into the instrumental CTIO system, $H_{\rm CTIO} = 21.29 \pm 0.05$. We stress that this indirect road NACO-IRSF-CTIO is actually the most accurate one to estimate the

Table 3. Photometric data for H CTIO, JHK IRSF, JHK NACO

Star ID	$H_{\rm CTIO}$	$H_{\rm IRSF,calib}$	$H_{\rm NACO,calib}$	$J_{\rm IRSF,calib}$	$J_{\rm NACO,calib}$	$K_{\rm IRSF,calib}$	$K_{\rm NACO,calib}$
1	16.95	13.094	13.106	13.872	13.855	12.88	12.898
2	17.69	13.834	13.826	14.230	14.225	13.77	13.76
3	-	14.340	14.352	14.83	14.884	14.24	14.246
target	-	-	17.47	-	18.068	-	17.349

instrumental magnitude in the CTIO system.

We also carry out the following independent check. We measure aperture fluxes f_i for stars 1, 2, 3, and the target listed in Table 3. For the target, we correct the result for contaminating flux from star 3 and from another much fainter nearby star. Then for each of stars $i = 1, 2, 3$, we obtain an estimate of the source-blend magnitude on the IRSF system: $H_{\mathrm{target};i,\mathrm{IRSF}} = H_{i,\mathrm{IRSF}} + 2.5\log(f_i/f_{\mathrm{target}})$. We take the average of these three estimates, and then apply the previously derived conversion from IRSF to CTIO. We find $H_{\mathrm{CTIO}} = 21.27$.

As a further sanity check, we apply a similar procedure to compare the NACO and CTIO images directly. As stated at the outset, we expect that this will be less accurate both because there are only two viable comparison stars (1 and 2) and because the CTIO flux measurements are less accurate than those of IRSF. Nevertheless, we find a similar result: $H_{\mathrm{CTIO}} = 21.32$ although with substantially worse precision.

We finally adopt $H_{\mathrm{CTIO}} = 21.28 \pm 0.05$, where the error bar reflects our estimate of the systematic error. Clearly, our two primary methods of estimating this quantity agree much more closely than this, but there still could be systematic effects common to both. We regard this error bar as moderately conservative.

7.3. Lens Mass Estimate

The best-fit wide and close planetary solutions give the same H-band model source flux, corresponding to $H_{\mathrm{source,CTIO}} = 21.56 \pm 0.05$ (error bar from the fit) on the instrumental CTIO system. Using the CTIO-IRSF-2MASS transformation, we find the calibrated H-band magnitude of the unmagnified source, $H_{\mathrm{source,2MASS}} = 17.75 \pm 0.05$. We use the time interval after the peak (19.19 days) divided by t_{E} (10.97 and 10.98 days for the close and wide solutions respectively) to determine the source/lens separation u at the time the NACO image was taken. Using the point-lens approximation, which accurately describes the wings of the light curve, the magnification at this separation is $A \sim 1.09$. Converting the magnified model source flux to the CTIO magnitude system, we discover that the light aligned with the target on the NACO image is ~ 0.19 mag brighter than the magnified light from the source. In principle, the blended light could be due to unrelated stars along the line of sight. However, the low density of such stars on the scale of the NACO resolution makes this very unlikely.

There remain three possibilities for the origin of excess light: the lens, a companion to the source, or a companion to the lens. We briefly argue that the first option is the most likely but the others are also quite viable, so that only future observations can distinguish

between these possibilities. First, as we calculate below, if the blended light is the lens, then the lens lies quite close to the source, which means that the received flux implies very similar stars in the first two cases. This means that the source-companion hypothesis is disfavored relative to the lens hypothesis by a factor ~ 0.5 (the fraction of turnoff stars with companions within the 500 AU resolution of NACO) but is favored by the higher optical depth of disk+bulge lenses (which are available if the lens is not specified) compared to bulge lenses (if the lens is specified to lie in the bulge). This factor would be about 1.5, if one could assume that bulge K dwarfs and disk brown dwarfs (which are the lens types in the two cases) are equally likely a priori to host planets with Saturn/Sun mass ratios. Actually, we have essentially no information on this question, which is the reason we refrain from a detailed analysis of relative probabilities.

The argument is similar when comparing the lens-companion versus lens hypotheses. In this case we are considering the probability of a microlensing event due to a companion of an observed (in blended light) K dwarf (assuming for the moment that the lens is in the bulge). Again the companion rate for K dwarfs within 500 AU is only about 50%. And again, a similar argument (and uncertainty) applies if the lens and its companion lie in the foreground disk.

The astrometric work shows the source displaced from the centroid of the target on the NACO image by 12.7 ± 5 mas. If this offset is real and is due to the detected blend, then the blend would have to be displaced ~ 70 mas from the source. This is within the FWHM of the target(140 mas along the major axis and 124 mas along minor axis of the elliptical Gaussian PSF), so such an offset is possible without being resolved in the NACO image. A displacement this size would rule out the lens as the source of excess light. However, we suspect the NACO image may suffer from distortions at the 10 mas level, so this is not compelling evidence of a separation between the source and blend. In addition, we note that such a displacement could occur by chance with 4% probability.

Assuming the blended light is due to the lens, we find $H_{\rm lens,2MASS} = 19.52^{+0.61}_{-0.39}$ and $M_{\rm H,lens} = 4.57^{+0.61}_{-0.39}$. We use a series of isochrones generated by the Dartmouth Stellar Evolution Database (Dotter et al. 2008) with [Fe/H] ranging from -0.5 to 0.5 and age ranging from 5 Gyr to 10 Gyr to estimate the lens mass $M_L = 0.69 \pm 0.14\,M_\odot$ and consequently the planet mass $m = 76 \pm 17\,M_\oplus$. This places the lens at a distance just 300 pc in front of the source, i.e, clearly in the bulge.

8. Discussion

Microlensing event MOA-2008-BLG-310 is one of only a few high magnification events to date for which the source is as large or larger than the central caustic. In this way, it bears many similarities to MOA-2007-BLG-400 (Dong et al. 2008). Like that earlier event, the planetary perturbations in the light curve are not immediately apparent, having been smoothed out by finite-source effects. We find that a Saturn mass ratio planet/star model is nevertheless favored over the single-lens model by a significant reduction in χ^2. Using VLT NACO and IRSF photometry, we obtain a possible estimate of the flux from the lens star, and so (assuming it is a main-sequence star) of its mass, $M_L = 0.69 \pm 0.14\,M_\odot$. Hence, the planet mass is below that of Saturn. We are not able to resolve the close/wide degeneracy in the binary geometry. However the separate solutions for the lens/star separation d differ only by a factor of 1.17. The $d \leftrightarrow -d$ degeneracy is not as severe in this case because the planet is located very close to the Einstein radius. This event is of particular interest in terms of understanding the abundance of planets in the Galaxy. Using a combination of color-magnitude data and model parameters, we are able to place some constraints on the lens mass and distance. We conclude that if the lens is a star, then it must be in the bulge.

MOA-2008-BLG-310Lb is the strongest candidate to date for a bulge planet. What are the prospects for confirming this candidate? As we discussed in § 6, the event contains essentially no parallax information. Hence, the only path toward confirmation that it is a bulge planet is direct detection of the host. For either the wide or close solution, the geocentric proper motion is $\mu_{\rm geo} = \theta_{\rm E}/t_{\rm E} = 5.4\,{\rm mas\,yr^{-1}}$. The heliocentric and geocentric proper motions differ by

$$|\boldsymbol{\mu}_{\rm hel} - \boldsymbol{\mu}_{\rm geo}| = |\mathbf{v}_{\oplus,\perp}|\pi_{\rm rel} = \frac{\theta_{\rm E}^2 v_{\oplus,\perp}}{\kappa M} = 0.019\,\frac{M_\odot}{M}\,{\rm mas\,yr^{-1}} \qquad (9)$$

where $v_{\oplus,\perp} = 28\,{\rm km\,s^{-1}}$ is the velocity of the Earth projected on the plane of the sky at the peak of the event. Hence, if the lens is luminous ($M \gtrsim 0.08\,M_\odot$), then the heliocentric and geocentric proper motions are essentially identical.

Thus, 10 years after the event, the lens will be separated from the source by $\sim 54\,{\rm mas}$, roughly the FWHM of a diffraction limited 8m telescope in H band. If light that is displaced from the source by 54 mas is observed at that time, it must be due to the lens or a companion to the lens (since a companion to the source would have the same proper motion as the source). If the lens emits 20% as much light as the source (our best estimate for the excess blended light) it should be visible at that time.

As just mentioned, such a detection would clearly show that excess light was associated with the lens rather than the source. But the question would still remain as to whether

the light so detected was from the lens itself or from a companion to the lens. A putative companion would generate a shear

$$\gamma = Q\Big(\frac{\theta_{\rm E}}{\Delta\theta}\Big)^2 \sim 10^{-5} Q\Big(\frac{50\,{\rm mas}}{\Delta\theta}\Big)^2 \tag{10}$$

where Q is the mass ratio of the putative companion to the lens and $\Delta\theta$ is their separation. From the smoothness of the residuals, one can place limits on the shear: $\gamma < 5 \times 10^{-4}$ would have easily been detected, and it is likely that a detailed triple-lens analysis would yield somewhat stronger limits. We already know that $\Delta\theta < 50\,{\rm mas}$, since otherwise the companion would have been seen in the VLT images. The hypothesis that the lens is not in the bulge requires that $M < 0.08\,M_\odot$, so depending on the flux measured from the newly detected object, one could place lower limits on Q. Therefore, it is quite possible that the detection of this light would prove that the lens was in the bulge. Even if it did not, a second epoch a few years later would measure the proper motion of the additional light and so place much stronger limits on $\Delta\theta$ at the time of the event. In brief, with a few years of patience, one should be able to determine whether the lens, and hence its planet, is in the bulge.

The procedure just outlined is challenging but alternative routes to secure detection of bulge planets are, if anything, more difficult. Gaudi (2000) discussed the prospects for detecting transiting planets in the bulge and Sahu et al. (2006) reported the detection of 16 candidate bulge planets from a transit survey carried out with the *Hubble Space Telescope*. Two of these were bright enough for radial-velocity follow-up, one of which showed variations consistent with a planet with mass $m = 10\,M_{\rm Jupiter}$ and the other showed upper limits $m < 4\,M_{\rm Jupiter}$. The stars are so bright, however, that their inferred masses indicate that at least one (and possibly both) probably lie in the foreground disk. Nevertheless, this technique could in principle be pushed harder, particularly when larger telescopes come on line. Even then, however, lower-mass planets, $m \lesssim M_{\rm Jupiter}$ will probably only be accessible with microlensing.

There are three other planets detected by microlensing for which the distances are neither measured nor strongly constrained, OGLE-2005-BLG-169Lb (Gould et al. 2006), OGLE-2005-BLG-390Lb (Beaulieu et al. 2006), and MOA-2007-BLG-400Lb (Dong et al. 2008). In all three cases, both $\theta_{\rm E}$ and μ are measured, so we estimate the minimum lens mass that would allow the lens-planet system to be in the bulge and the time that must elapse before definitive imaging observations can be undertaken.

For OGLE-2005-BLG-169Lb, $\theta_{\rm E} = 1.00 \pm 0.22\,{\rm mas}$ and $\mu = 7 - 10\,{\rm mas\,yr^{-1}}$. Even adopting the $1\,\sigma$ lower limit on $\theta_{\rm E}$, then $\pi_{\rm rel} > 75\,\mu{\rm as}$ for stellar hosts with $M \geq M_\odot$. Thus, for bulge sources at $D_{\rm s} = 8\,{\rm kpc}$, the lens distance is no more than 5 kpc. Hence, the lens is almost certainly in the disk. Measurements to confirm this relatively secure conclusion

could be made as early as 7 years after the event, i.e., 2012.

For MOA-2007-BLG-400Lb, $\theta_{\rm E} = 0.32 \pm 0.02\,{\rm mas}$ and $\mu = 8.2 \pm 0.5\,{\rm mas\,yr^{-1}}$. Adopting $D_{\rm s} = 8\,{\rm kpc}$, the lens would only lie within 2 kpc of the source provided that $M \gtrsim 0.30\,M_\odot$. Thus, this is a reasonable, but not particularly strong candidate for a bulge lens. The source is a moderately bright subgiant, so for 10m class telescopes it is perhaps best to wait for the separation to reach 70 mas, which will require about 9 years, i.e., in 2016.

Finally, OGLE-2005-BLG-390Lb, has $\theta_{\rm E} = 0.21 \pm 0.03\,{\rm mas}$ and $\mu = 6.8 \pm 1.0\,{\rm mas\,yr^{-1}}$. It is therefore the best previous candidate for a bulge lens since $\theta_{\rm E}^2$, which is the product of the mass and relative parallax, is only a factor 1.6 times larger than for MOA-2008-BLG-310Lb. This means that if it were at the bottom of the main-sequence, it would lie about 3 kpc in front of the source and therefore most likely lie in the disk, but if it had significantly larger mass it would be in the bulge. However, in this case, the source is a G4 III giant with $I_0 = 14.25$, which implies $M_H \sim -0.85$. A lens close to the bottom of the main sequence has $M_H \sim 11$ and so (even accounting for its closer distance) would appear 25000 times fainter than the source. While this is an extreme case, it would appear prudent to wait for the lens to move 3 FWHM away from the source, which for 10m class telescopes would require about 20 years, i.e. 2025. If larger telescopes with AO come on line before that, it will of course be possible to make the measurement sooner.

Many talented people contributed time and expertise to this work. I would like to thank Andy Gould and Scott Gaudi for coordinating the efforts of our collaborators and helping me prepare the manuscript. The code used to fit light curve models was designed by Subo Dong, my indispensable mentor for much of the modeling process. The μFun data reduction pipeline is maintained by Rick Pogge, who aided me with the earliest reductions for this event. Additional DIA reductions and astrometric work were contributed by Szymon Kozłowski. J.-P. Beaulieu and Taka Sumi obtained the NACO and IRSF images and undertook the complicated procedure for measuring light blended with the source. I am grateful to the members of the μFUN, MOA, MiNDSTEp, and PLANET collaboratons who provided the observations that made the analysis of this event and the discovery of a planet possible.

This work was supported in part by the Summer Undergraduate Research Program at the OSU Department of Astronomy, and by an allocation of computing time from the Ohio Supercomputer Center.

REFERENCES

An, J.H. et al. 2002, ApJ, 572, 521

Beaulieu, J.-P. et al. 2005, Nature, 439, 437

Bennett, D.P. et al. 2008, ApJ, 684, 663

Bennett, D.P., Anderson, J., & Gaudi, B.S. 2007, ApJ, 660, 781

Bessell, M. S., & Brett, J. M. 1988, PASP, 100, 1134

Bond, I.A., et al. 2004, ApJ, 606, L155

Chung, S.-J. et al. 2005, ApJ, 630, 535

Claret, A. 2000 A&A, 363, 1081

Cohen, J.G., Thompson, I.B, Sumi, T., Bond, I., Gould, A., Johnson, J.A., Huang, W., Burley, G. 2009, ApJ, in press (arXiv:0904.2020)

Devillard, N. 1997, The Messenger, 87, 19

Devillard, N. 1999, Astronomical Data Analysis Software and Systems VIII, 172, 333

Diolaiti, E., Bendinelli, O., Bonaccini, D., Close, L., Currie, D., & Parmeggiani, G. 2000, Astronomical Data Analysis Software and Systems IX, 216, 623

Dong, S. et al. 2008, ApJ, in press (arXiv:0809.2997)

Dong, S. et al. 2009, ApJ, in press (arXiv:0804.1354)

Dotter, A., Chaboyer, B., Jevremović, D., Kostov, V., Baron, E., & Ferguson, J. W. 2008, ApJS, 178, 89

Gaudi, B.S. 2009, Astronomy, 2010, 85

Gaudi, B.S. 2000, ApJ, 539, L59

Gaudi, B. S., et al. 2008, Science, 319, 927

Gould, A. 1994, ApJ, 421, 71

Gould, A. 2000, ApJ, 542, 785

Gould, A. et al. 2006, ApJ, 644, L37

Griest, K. & Safizadeh, N. 1998, ApJ, 500, 37

Han, C. 2005, ApJ, 633, 414

Han, C. 2007, ApJ, 661, 1202

Hardy, S.J. & Walker, M.A. 1995, MNRAS, 276, L79

Kervella, P., Thévenin, F., Di Folco, E., & Ségransan, D. 2004, A&A, 426, 297

Kiraga, M. & Paczyński, B. 1994, ApJ, 430, L101

Poindexter, S., Afonso, C., Bennett, D. P., Glicenstein, J.-F., Gould, A., Szymański, M. K., & Udalski, A. 2005, ApJ, 633, 914

Pollack, J. B., Hubickyj, O., Bodenheimer, P., Lissauer, J. J., Podolak, M., & Greenzweig, Y. 1996, Icarus, 124, 62

Sahu, K.C. et al. 2006, Nature, 443, 534

Schechter, P.L., Mateo, M. & Saha, A. 1993, PASP, 105, 1342

Smith, M.C., Mao, S., & Paczyński, B. 2003, MNRAS, 339, 925

Udalski, A., et al. 2005, ApJ, 628, L109

Woźniak, P.R. 2000, Acta Astron., 50, 421

Yoo, J. et al. 2004, ApJ, 603, 139

.

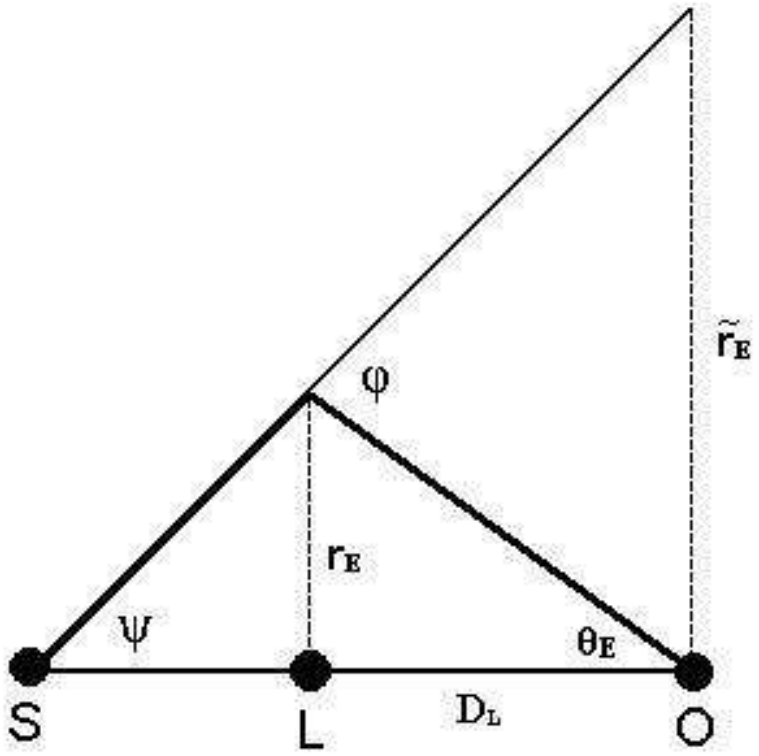

Fig. 1.— Basic geometry of microlensing. the source is S, lens L, and observer O. Light from the source is bent through angle ψ. The physical Einstein radius, r_E, is the radius at which light from the source is bent directly toward the observer when the source and lens are exactly aligned. The angular size of the Einstein radius is θ_E and the Einstein radius projected into the plane of the observer is $\tilde{r}_E$. The distance to the lens is D_L.

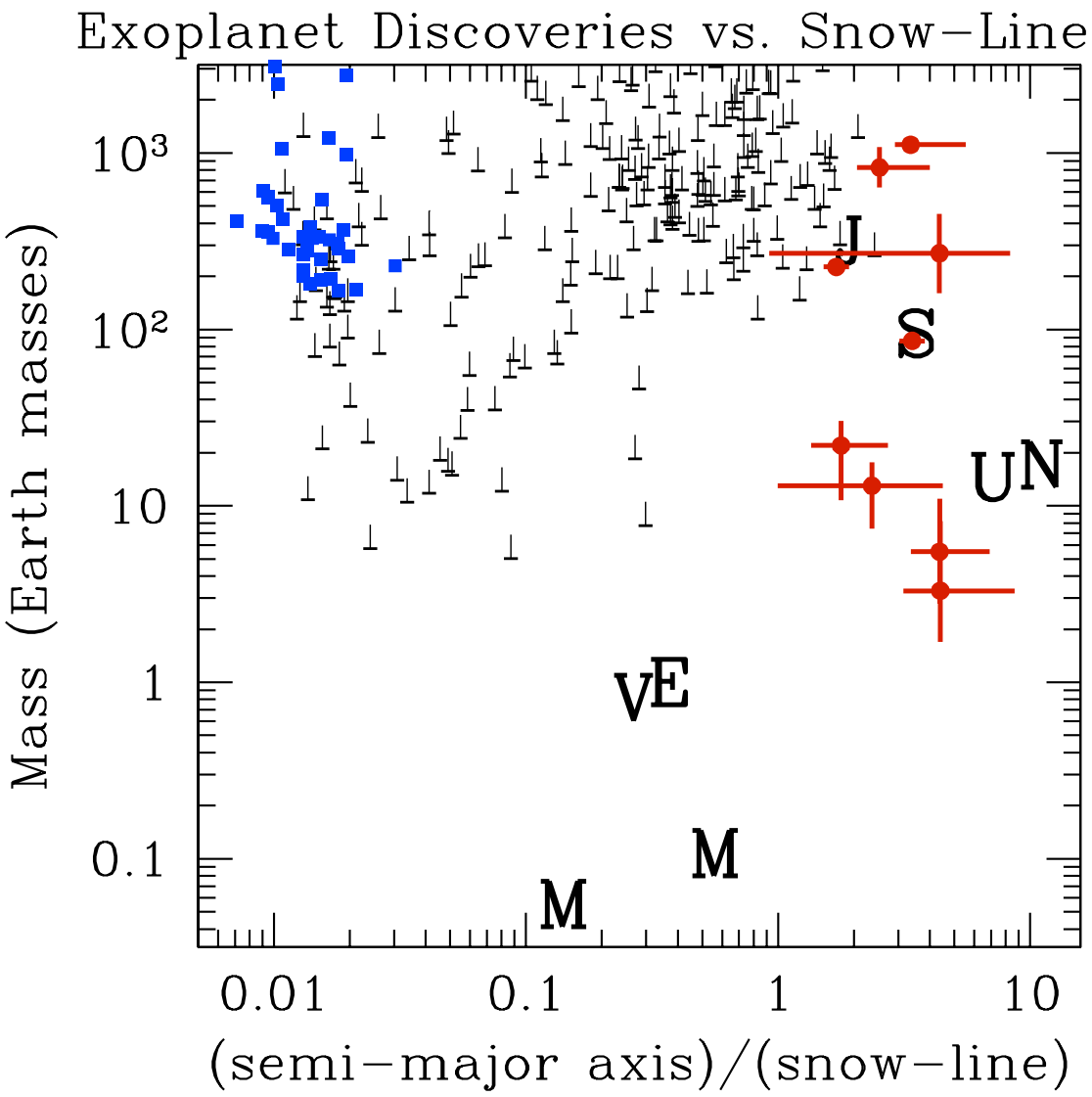

Fig. 2.— Plot of mass vs. seperation from host star relative to the Snow Line for planets detected via transits (*blue*), radial velocities (*black*) and microlensing (*red*). Microlensing is probing regions beyond the Snow Line that other methods are insensitive to. (Figure from Gaudi 2009)

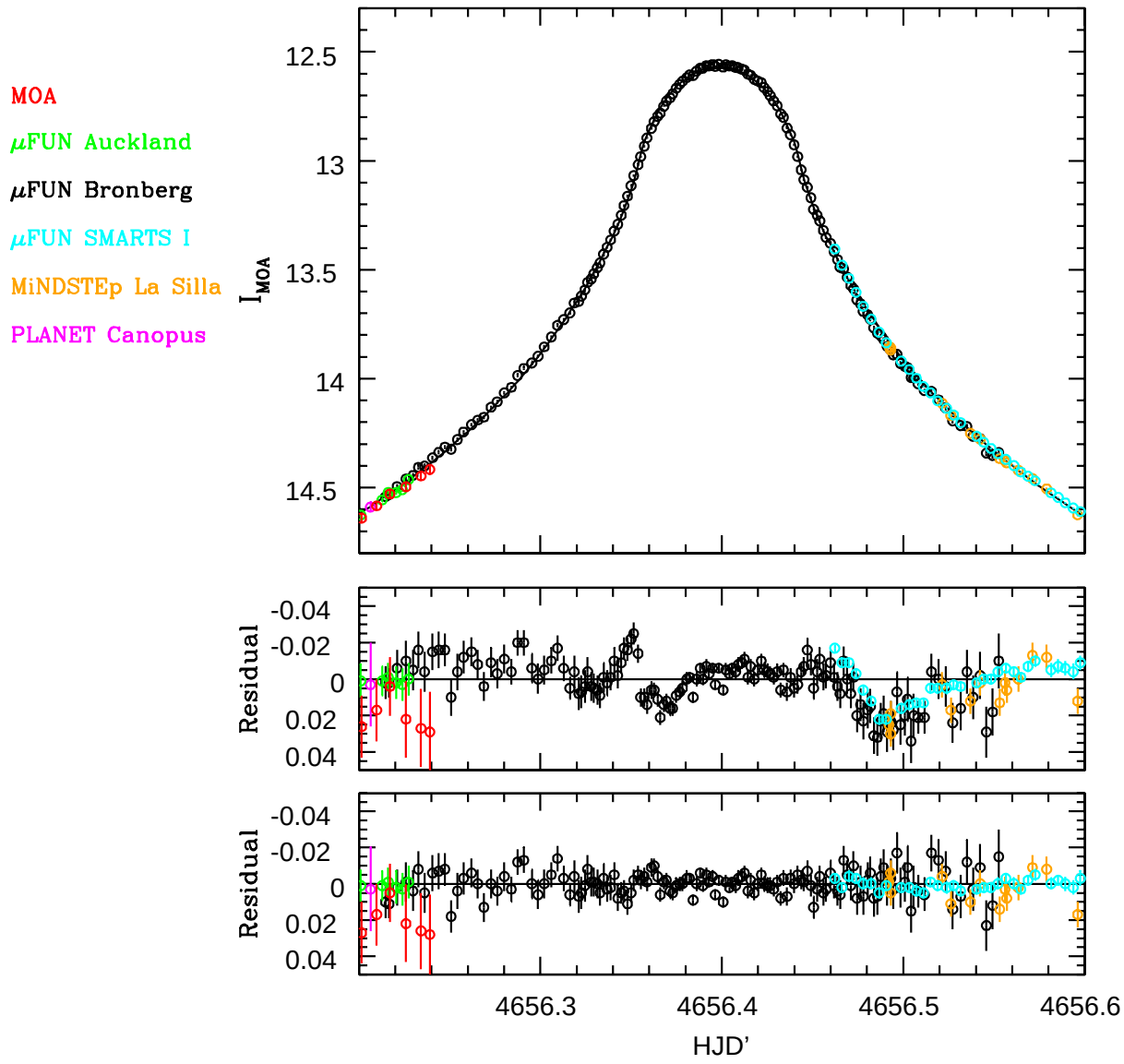

Fig. 3.— Top: Lightcurve of MOA-2008-BLG-310 showing data from MOA (*red*), Auckland (*green*), μFUN Bronberg (*black*), μFUN SMARTS *I*-band (*cyan*), MiNDSTEp La Silla (*orange*), and PLANET Canopus (*magenta*). The lightcurve does not look anomalous at first glance. The data are approximately calibrated to the MOA magnitude scale. Middle: Residuals to the best fit single-lens model. Anomalies are apparent at HJD′ = 4656.34 and HJD′ = 4656.48. Bottom: Residuals to the best fit planetary model (the wide solution is chosen for this plot, however the close solution is nearly indistinguishable).

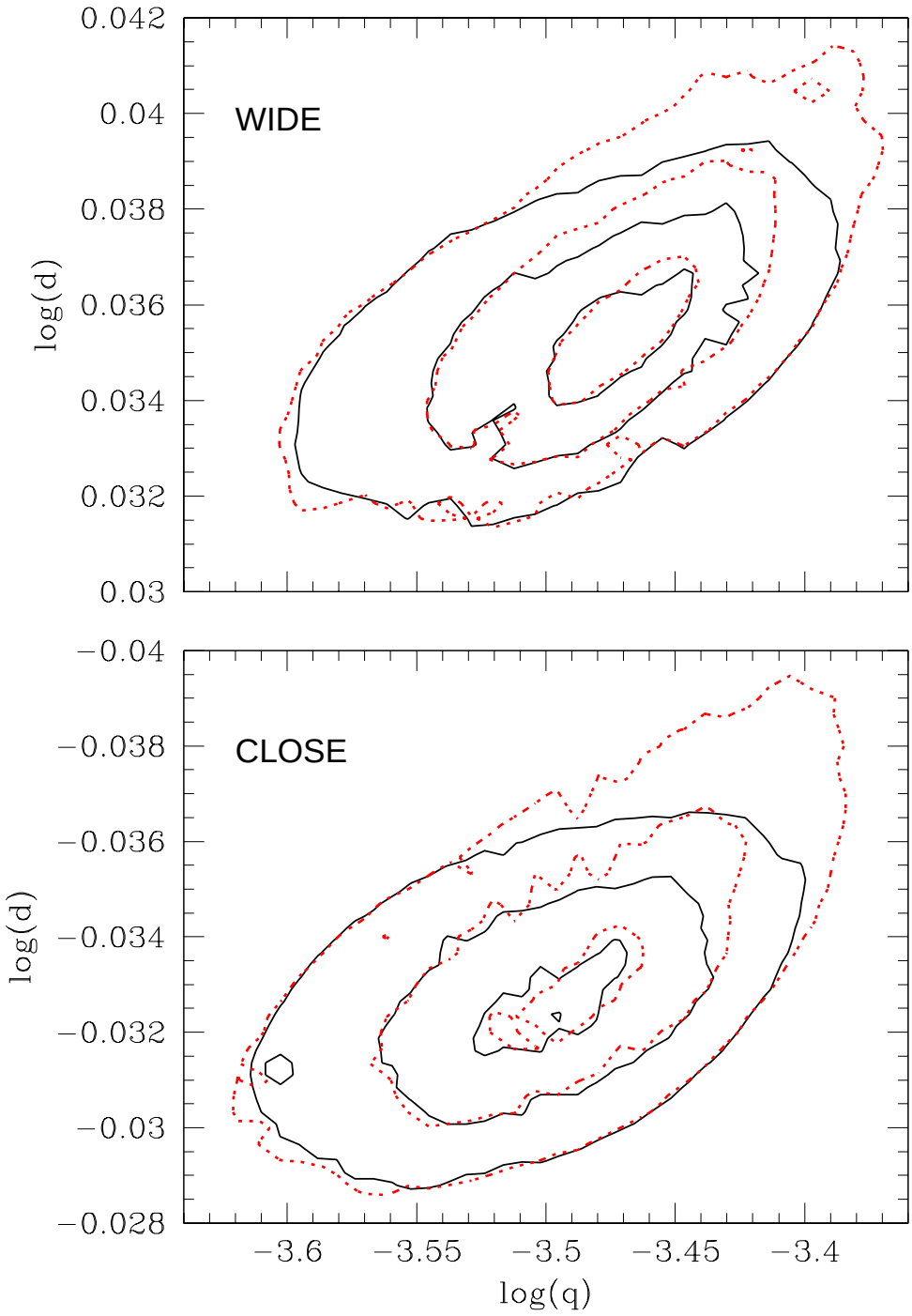

Fig. 4.— Top: The wide solution $\Delta\chi^2 = 1, 4, 9$ contours in the (d, q) plane. The contours generated by fixing the limb darkening parameters at the Claret (2000) values (*solid black lines*) are similar to those from allowing Γ and Λ to vary freely (*dotted red lines*). Large regions of the $\Delta\chi^2 = 1$ minima overlap. Bottom: $\Delta\chi^2$ contours for the close solution.

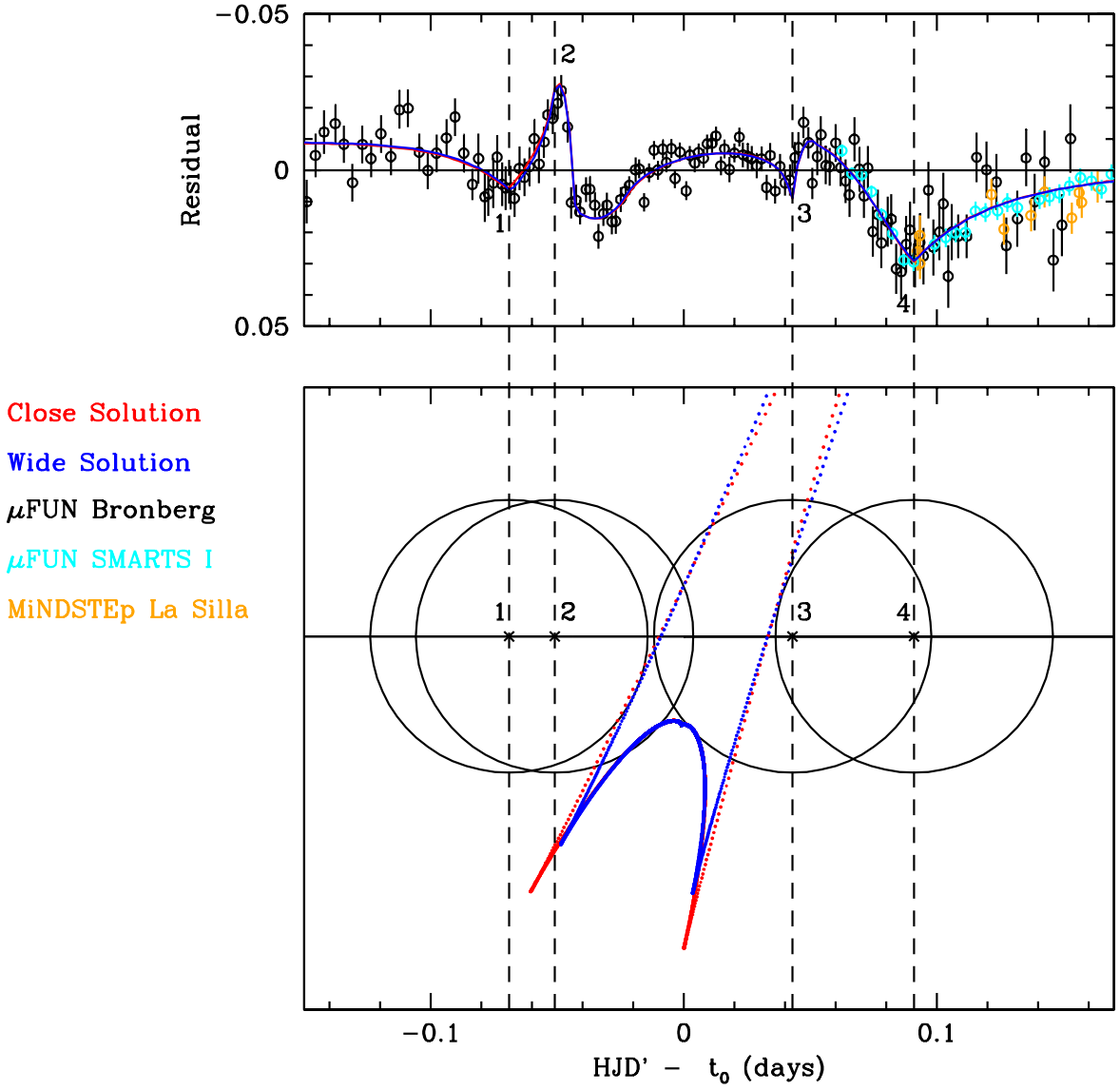

Fig. 5.— Top: Residuals to the best fit single-lens model. Data points are shown for μFUN Bronberg (*black*), μFUN SMARTS (*cyan*), and MiNDSTEp La Silla (*orange*). The solid lines are the best fit wide (*blue*) and close (*red*) planetary models. Bottom: The extended source (*circle*) is shown at key points in time along its trajectory (*solid black line*). The caustics for the wide and close models are plotted in blue and red, respectively. Solid lines correspond to stronger magnification while dotted lines indicate that the caustic is weaker. The two caustic structures are nearly indistinguishable in regions probed by the source. Several anomalous features of the residual plot correspond to the limb of the source crossing the caustic. These features are numbered, and dashed black lines connect them to the corresponding position of the source.

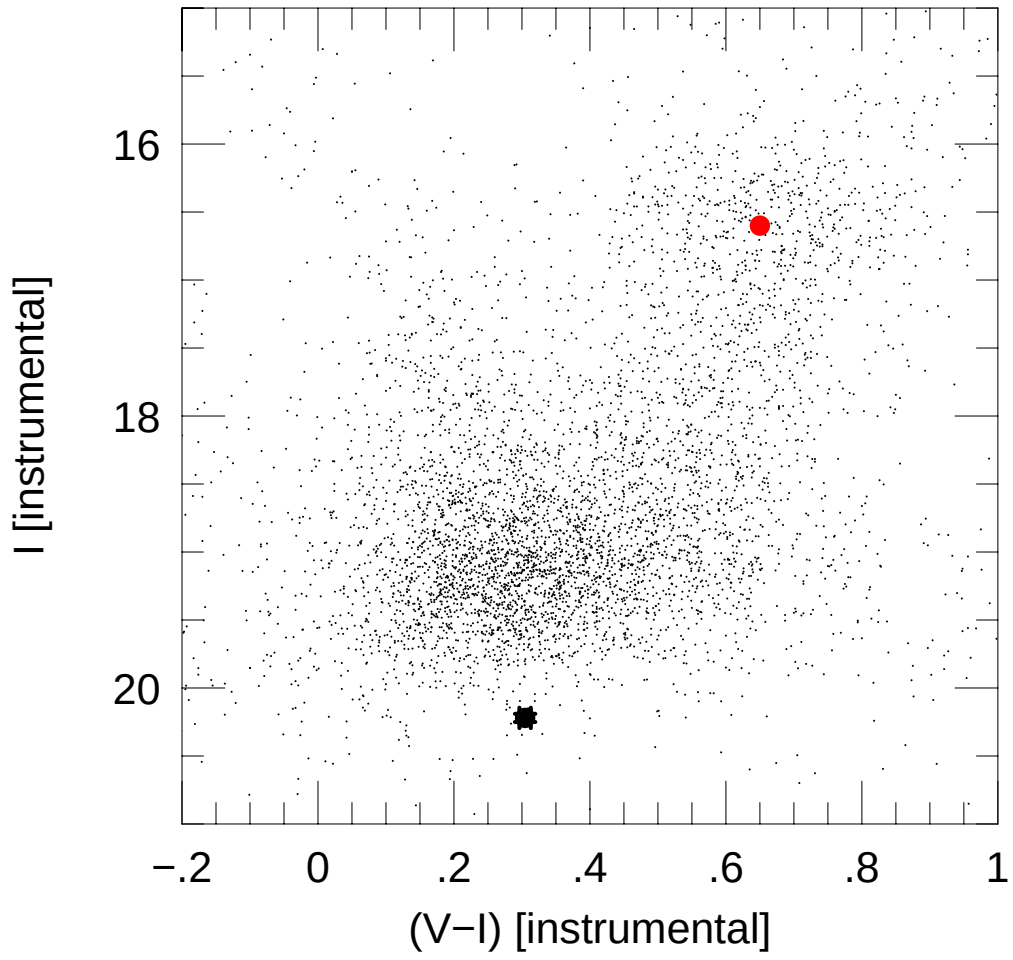

Fig. 6.— Instrumental color-magnitude diagram of the field containing MOA-2008-BLG-310. The clump centroid is indicated in red. The source color and magnitude (*black*) is derived from the best-fit close binary model. We estimate the offset to the clump $\Delta[(V-I), I] = (-0.35, 3.62)$. Assuming the source lies at 8 kpc, $(V-I)_0 = 0.70$ and $M_I = 3.4$, consistent with a post-turnoff G type star.

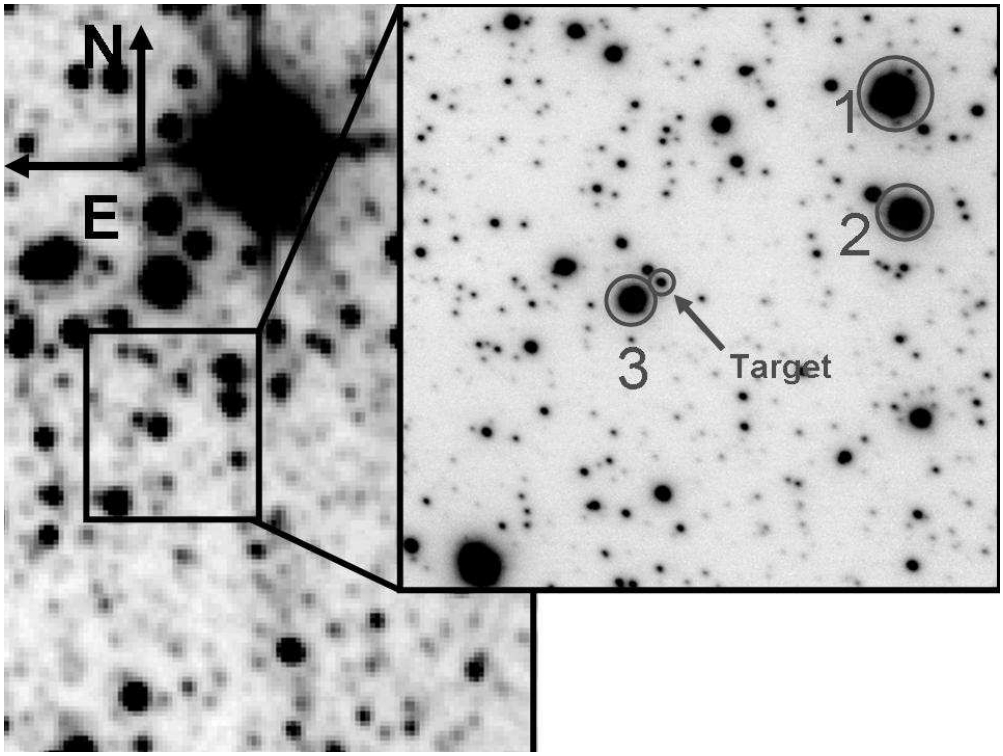

Fig. 7.— Left: The median H-band AO image taken by NACO on VLT near the baseline of the event. Right: Zoom of NACO image with the lensed source plus blend (target) and reference stars circled.